Four-Dimensional Analysis Experiment During the Gate Period Part II

K. MIYAKODA, J. SHELDON AND J. SIRUTIS

Geophysical Fluid Dynamics Laboratory/NOAA, Princeton University, Princeton, NJ 08540

(Manuscript received 31 August 1980, in final form 3 November 1981)

ABSTRACT

The GATE analysis was repeated utilizing the full GATE data set in the delayed mode and a revised four-dimensional analysis procedure. The resulting maps were compared with maps of other authors. Based on the new analysis, macroscale circulation features for the tropical African continent and Atlantic Ocean region were calculated, and other characteristic phenomena of this area were investigated. The easterly waves, in particular, were studied with respect to their formation, propagation, associated condensation, and possible conversion to hurricanes. It was possible to trace nine distinct easterly waves throughout their entire life history, and the analyzed tracks of these easterly waves agreed quite well with the subjective analyses of Sadler and Oda (1978). The time sequences of precipitation over the GATE A/B-array obtained by the present analysis and by satellite estimates were compared with some success.

1. Introduction

The 101-day sequential map analysis of the GATE data was first conducted at GFDL in 1974 on a near-real time basis, using the four-dimensional analysis method (Part I: Miyakoda *et al.*, 1976). Although the data coverage over the Atlantic Ocean was unprecedently good, the data received on a real-time basis at the National Meteorological Center (NMC), Washington, DC, through the GTS (Global Teleconnection System) was not entirely satisfactory, particularly with regard to the GATE-dedicated ship data, station data over the African Continent, and commercial aircraft reports. In addition, the analysis technique used in 1974 proved to be too insensitive to reproduce smaller-scale disturbances; i.e., a horizontal scale of 600–3000 km.

In 1978–79, the GATE analysis was repeated with a revised analysis method for the 34-day period from 20 August–22 September, which includes Phase III of GATE. An expanded data set was used which was processed and validated in a delayed mode and included the supplemental data. The number of observations in the final GATE data set (first available in 1977) was substantially increased compared with that of the near-real-time Level II-b data set. (Upper air: 34%; surface: 22%; ship: 50%). As a consequence, the final results of analysis have been noticeably improved. The objective of this paper (Part II) is to present some of the highlights of the summer 1974 tropical circulation and phenomena in the GATE area, as were revealed in the new four-dimensional analysis, and to review the quality of the analysis.

Although there is some disagreement over terminology regarding tropical disturbances, it is, after all, largely an exercise in semantics. So, to avoid confusion, we shall, for the purposes of this paper, consider an "easterly wave" to be any traveling disturbance possessing a distinct vorticity maximum and having time continuity, regardless of origin or whether or not there is a closed circulation.

2. Analysis scheme and examples

a. 1978–79 version of the four-dimensional analysis

The procedure used here is an early version of the FGGE analysis systems at GFDL. It consists of both a dynamical assimilation and a static analysis. The principal difference from the 1974 version is that the static analysis is applied at 12-hour intervals and the dynamical assimilation is re-started from this static analysis.

The first step is the preparation of insertion data for the model. Values are determined at the model's gridpoints using a univariate optimum interpolation analysis method (Gandin, 1963; Alaka and Elvander, 1972) with a data collection range of 250 km around a gridpoint and using the climatological normal as the initial guess. The dynamical data assimilation (4DA) is based on the system developed primarily by Simmonds (1978), using a spectral method. After each 12 h period of assimilation, the global optimum interpolation analysis (OPA) is applied, this time using the 4DA result as the initial guess and an expanded data collection range of 500 km. This static analysis is the final adjustment of Level III data to Level II data, substantially eliminating the model's

bias and making an optimal fit of the analysis to the original observations, although this is not without the loss of some dynamical consistency.

The basic GCM (general circulation model) used in the assimilation is a global spectral transform model with a spherical harmonic representation in the horizontal, and finite difference formulation in the vertical (Gordon and Stern, 1974). The spectral resolution of the model is R30L9, which denotes the rhomboidal 30-harmonic truncation and nine vertical levels. The model physics are virtually identical to that of the GFDL 1965 version (see the A2-physics in Miyakoda and Sirutis, 1977) and are not the most sophisticated physics available. Some key aspects of the physics are as follows: the cumulus cloud effect is modeled by the "moist convective adjustment" (Manabe *et al.*, 1965); the subgrid scale eddy viscosity is incorporated through the linear ∇^2 formulation for temperature and mixing ratio of water vapor and a form of divergence damping; cloud-radiation interaction was not included; and diurnal variability was not considered. (However, the observed data should include the effect of diurnal variability implicitly). In addition to the normal physical processes incorporated in the A2 physics, this version of the GCM carries soil moisture as a variable, and also includes a snow–albedo feedback effect.

The spectral transform model has 96 grid points per row and 80 rows from pole to pole which corresponds to a longitudinal grid distance $\Delta\lambda = 3.75°$ and the meridional grid distance $\Delta\phi = 2.4°$.

One significant difference between this version and Part I is that the GCM used in Part I was a finite difference model on the so-called "modified Kurihara" grid (see Part I), with a resolution designated as N48L9. This denotes a grid with 48 points from pole to equator and nine vertical levels. The longitudinal resolution varies from $\sim 1.9°$ at the equator to 10° near the pole. This implies that there is a significant drop in longitudinal resolution in the new version (although a strict comparison between a grid-point model and a spectral model is difficult). The spectral model was chosen, despite this disadvantage, because of its significantly greater economy. Also, it was assumed that a good deal of the smaller scale information would be restored during the static analysis, which was done on the modified Kurihara grid.

There were other differences between the two analyses, also. In Part II, the data are inserted at each of the levels, including the planetary boundary layer, whereas data in the lowest two levels were not utilized at all in Part I. Moisture data, not considered in Part I, was included this time by virtue of the static analysis, and the semi-implicit time differencing method is used with a divergence damping in the spectral model, whereas Euler backward time differencing was employed in Part I.

The products of the global OPA are V, T, q and z at the 19 standard pressure levels as well as pressure and temperature at sea level, P_{SL} and T_{SL}. In addition, the model produces data on the precipitation rate (RC), soil moisture, (SM), short- and long-wave radiation, (I and $F\downarrow$), snow and ice coverage and depth, ($S + I$), surface wind stress, (τ_x and τ_y), etc.

Let us first look at some examples of the global maps produced by these two four-dimensional analysis systems. Fig. 1 is a comparison of the streamline and isotach charts at 00GMT, September 6, 1974, from Part II and Part I. It is interesting to note that both analyses capture Hurricane Carmen over the Yucatan Peninsula (90°W, 23°N), Typhoon Shirley south of Japan (125°E, 25°N), and Tropical Depression Elaine north of Venezuela (58°W, 18°N). Surprisingly, the two maps show a great deal of resemblance in the overall features, despite the different analysis techniques and different volume of data employed. But there are also noticeable differences in the 850 mb map. Easterly waves are better represented over Africa and Atlantic, and the streamlines are smoother. The easterly wave destined to become Hurricane Fifi was located over Africa at this time, and is much better defined in the new analysis. In general, the troughs and ridges in the extratropics are deeper than in Part I. The East African Jet (EAJ) is more meridionally oriented in the new version and the streamlines over the southern hemisphere differ substantially from those in the previous analysis.

b. Effect of spatial resolution on the analysis

In the previous study (Miyakoda *et al.*, 1974), it was tentatively concluded that, for the tropical analysis, a grid interval of <2° would be needed, especially with regard to these small scale, low-level vortices (mean wavelength 2500 km). In an attempt to evaluate the effect of spatial resolution, the OPA analysis was repeated at various resolutions, specifically $\Delta\lambda\Delta\phi = 2°$, 1° and 0.5°, where the initial guess fields in all cases were derived from the 4DA of the R30L9 spectral model.

Fig. 2 shows the streamline maps produced from three versions of the OPA using these three resolutions. A subjective analysis made by Dean and Smith (1977) from the GATE A/B-scale area is shown for reference. In the three GFDL maps, the easterly waves are indicated by numbers 4, 5 and 6, following the numbering convention set by Sadler and Oda (1978). (Referred hereafter to as the S-O numbering system). Wave 6 has just moved off the African coast into the Atlantic. The observed wind data are plotted; they consist of the conventional World Weather Watch observations as well as specially prepared cloud winds and GATE ship data.

Overall, the three maps are quite similar to each other, but the charts for analyses using 1° and 0.5°

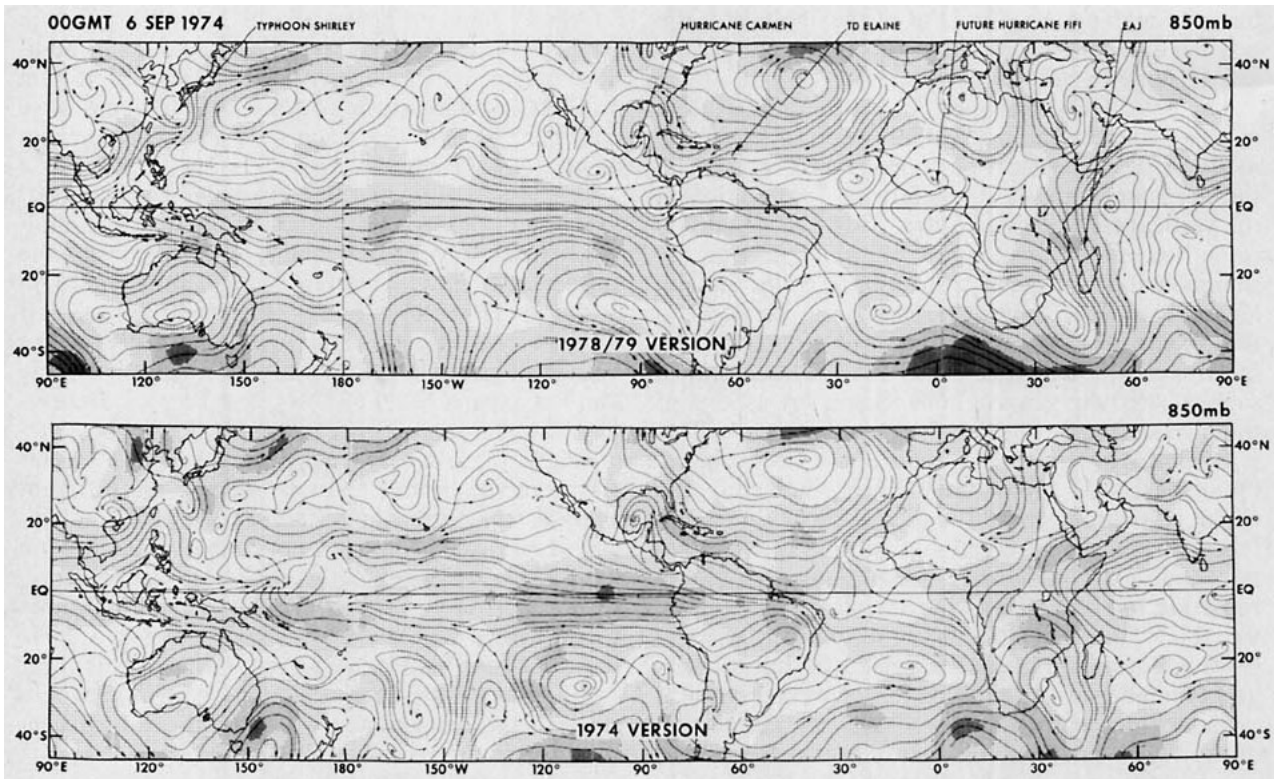

FIG. 1. 850 mb streamlines and isotachs for the 1978–79 (upper) and the 1974 (lower) versions. Regions with wind intensity greater than 5, 10 and 15 m s^{-1} are shaded light, medium, and dark, respectively.

resolution do display a somewhat sharper representation of waves 4 and 5 than does the 2° resolution map. All three conform quite closely to the available data. Differences with the subjective analyses occur mainly in regions without sufficient data to determine which is more correct, and so represent the difference between the analyzer's and model's view of continuity. In any case, it appears that when using the 4DA result from an R30L9 spectral model as a first guess, the effect of spatial resolution in the sub-

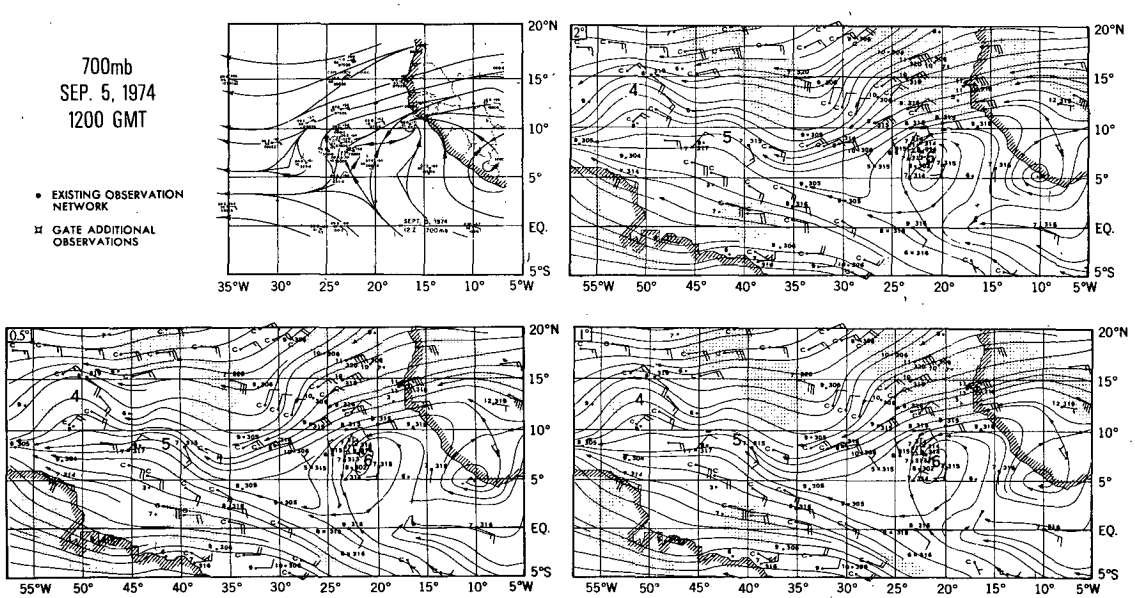

FIG. 2. The effect of spatial resolution on the analysis. Shown are optimum interpolation analyses based on 2, 1, and 0.5° resolution. "C" indicates a cloud wind. In the upper left is the hand analysis by Dean and Smith (1977).

sequent global optimum analysis is minimal. We feel, however, that if the first guess field were of higher resolution, the effect of higher spatial resolution in the static analysis would be enhanced.

c. *Comparison with other analyses*

The 1978–79 version of the GFDL four-dimensional analysis will now be compared with those of Pasch *et al.* (1978), Sadler and Oda (1978), Dean and Smith (1977), and objective analyses produced by the United Kingdom Meteorological Office (Jones, 1976; Reynolds, 1977). Shown below is a comparison over the GATE A-scale with the subjective analysis of Sadler and Oda, and a comparison with those of Dean and Smith over the A/B-scale area.

1) A-SCALE AREA

The 250 mb streamlines for 5 September, 1200 GMT are shown in Fig. 3 for both the GFDL and Sadler-Oda analyses. This is an appropriate level for comparison because of the relative abundance of observations there, e.g., aircraft reports and cloud-wind data. The analyses are quite similar in certain areas, such as the United States, the Atlantic Bight, Mexico, the Caribbean, West Africa and over the GATE A/B-scale area. Hurricane Carmen was located north of the Yucatan peninsula and the associated anticyclonic flow can be seen in both maps. Some differences can be seen over the north-central Atlantic and in the equatorial regions. In particular, the GFDL analysis tends to interpret the anticyclones rather as a series of separate smaller cells. It should be noted that obtaining an accurate wind analysis is extremely difficult at this level in equatorial regions (Gordon *et al.*, 1972).

Fig. 4 is a comparison of the GFDL and Sadler-Oda charts at lower levels. The atlas compiled by Sadler and Oda provides composite maps of surface flow over sea and 850 mb flow over land. The GFDL maps at 850 and 1000 mb are shown separately at the top and bottom, respectively, with the Sadler-Oda composite in the middle. The S-O numbering system has been adopted in identifying the low level vortices, starting with 2 (Hurricane Carmen) and proceeding through waves 4, 5, 6 and 7. Wave 3 had disappeared by this time. Wave 7, now located at 5°E over the African continent, will become Hurricane Fifi 11 days hence.

The agreement between these maps appears excellent, particularly with respect to the position of

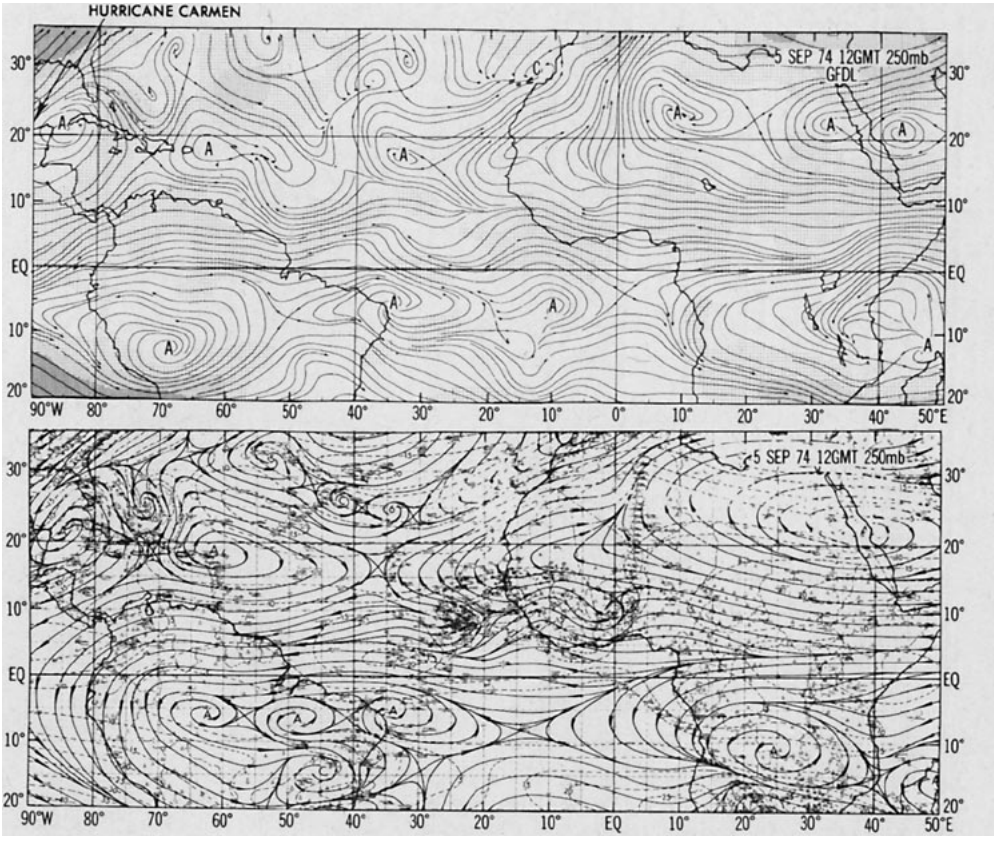

FIG. 3. 250 mb streamlines and isotachs for the GFDL, 1° resolution (upper) and Sadler and Oda (1978) (lower) analyses. In the GFDL map, regions with wind speeds greater than 10 m s^{-1} are stippled.

the disturbances. The principal discrepancy lies in the interpretation of the structure of the individual easterly waves, such as 4 and 5, Sadler-Oda's analysis displaying a more marked eddy-like nature in comparison to GFDL's broader, open-wave character. As was mentioned in the previous subsection, the 4DA was performed by the R30L9 spectral model, and the limited resolution involved might be responsible for this deficiency.

2) A/B-SCALE AREA

Fig. 5 shows a comparison over the smaller area between the GFDL analysis using 1° resolution in the OPA and the analysis of Dean and Smith (1977). The 250, 850, and 1000 mb maps are shown here, and the 700 mb pattern can be seen in Fig. 2. The agreement is reasonably good, even for some of the smaller-scale features. For example, the cyclonic-

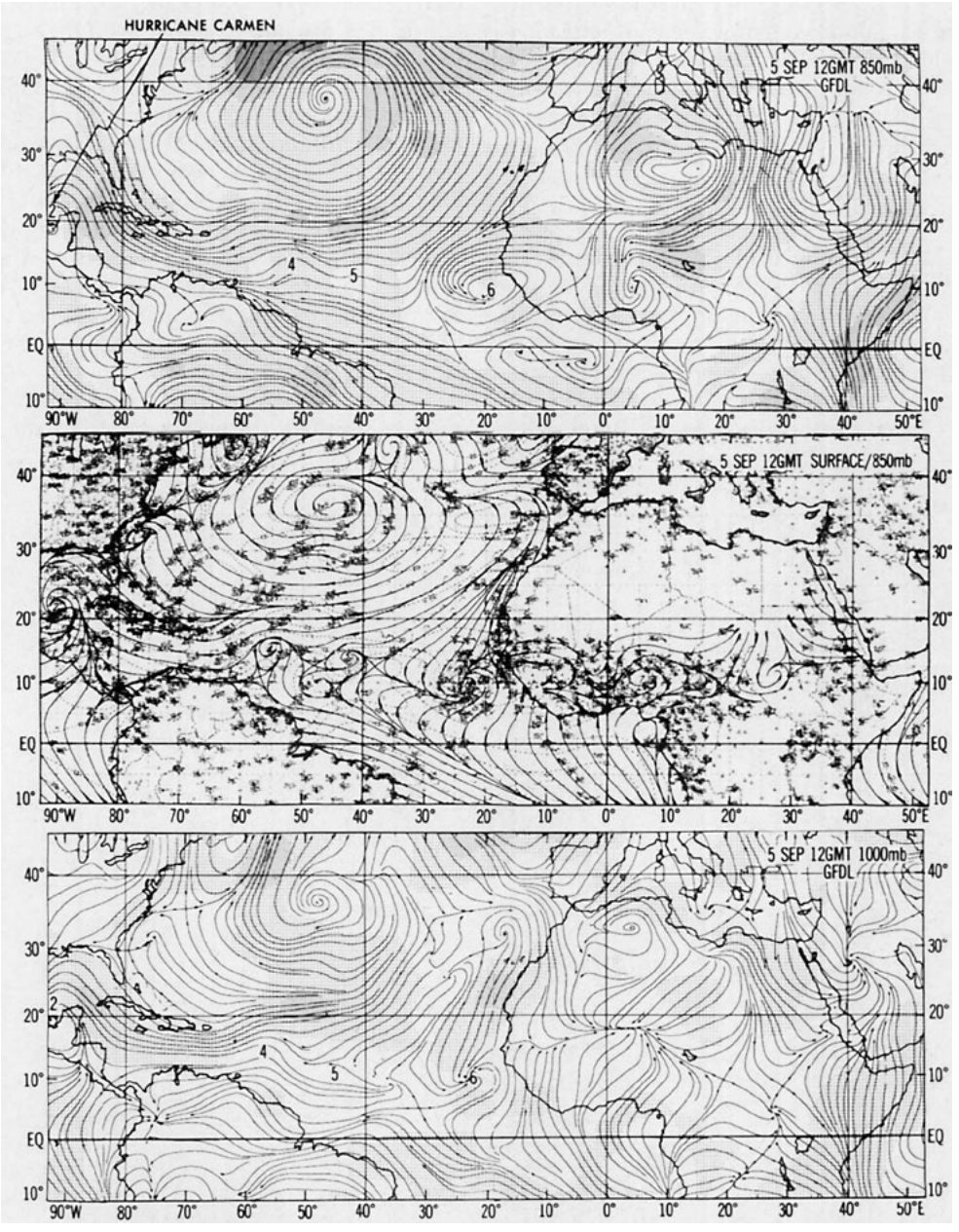

FIG. 4. Streamline maps of 850 mb flow for the GFDL analysis (upper), Sadler-Oda's composite of surface flow over sea and 850 mb flow over land (middle), and 1000 mb flow from the GFDL analysis (lower). In the GFDL analyses, regions with wind speeds in excess of 5, 10, and 15 m s^{-1} are shaded light, medium, and dark, respectively.

anticyclonic couplet noted in earlier studies (Carlson, 1969; Reed *et al.*, 1977) is evident in both analyses.

3. Macroscale features

Using the 1978/79 version of the analysis the mean structure of the atmosphere over the GATE A-scale area was studied by averaging variables over the 21-day period of GATE Phase III, covering the period from 0000 GMT 30 August to 1200 GMT 19 September. The parameters selected to depict this mean state are: wind, vorticity, vertical velocity, temperature, humidity, and precipitation, as represented in the analyses.

a. Horizontal maps

1) STREAMLINES AND ISOTACHS

The 200 mb flow field (top of Fig. 6) is characterized by two quasistationary planetary-scale features, i.e., the mid-Atlantic trough (MAT) and the subtropical ridge. The axes of these two features have a clear tilt from northeast to southwest, as was pointed out by Krishnamurti (1971). The tip of the trough reaches the West Indies, and protrudes into the anticyclone over the Caribbean Sea. The subtropical ridge extends from Tibet or eastern China to Africa, passing over the northern tip of the A/B-array at 15°N, and reaching to the middle of the Atlantic Ocean. To the south of the ridge is the upper tropospheric easterly jet, which has maxima over East Africa, the west African coast, and southwest of Latin America. The difluent wind axis over the A/B-array is located at 10°N, and agrees well with the results of Reynolds (1977), and Sadler (1975) who used aircraft data from 1963–73 in constructing his streamline maps. However, the placement of a col in the anticyclonic cell at 4°S, 8°E in the Southern Hemisphere is quite different from Sadler's and Reynolds' maps.

At 700 mb (middle of Fig. 6), a trough in the midlatitude westerlies lies beneath the mid-Atlantic

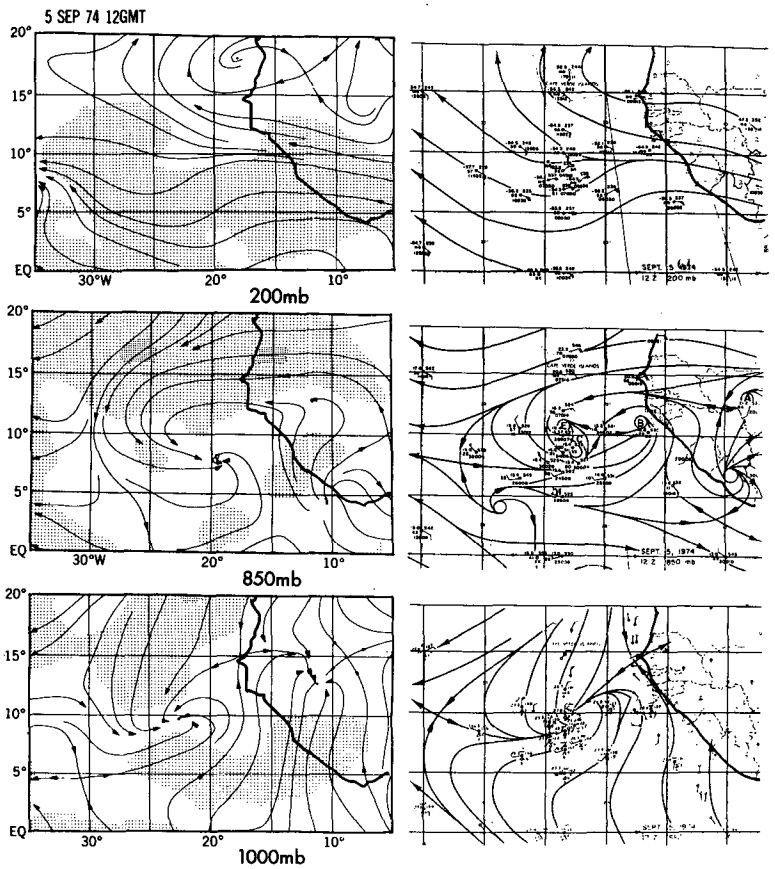

FIG. 5. Streamline and isotach maps at 200, 850 and 1000 mb for the GFDL, 1° resolution (left) and Dean-Smith (1977) (right) analyses. For the GFDL maps at 200 mb, regions with wind speeds greater than 10 m s^{-1} are lightly shaded. For the 850 and 1000 mb maps, regions with wind speeds greater than 5 and 10 m s^{-1} are shaded light and dark, respectively.

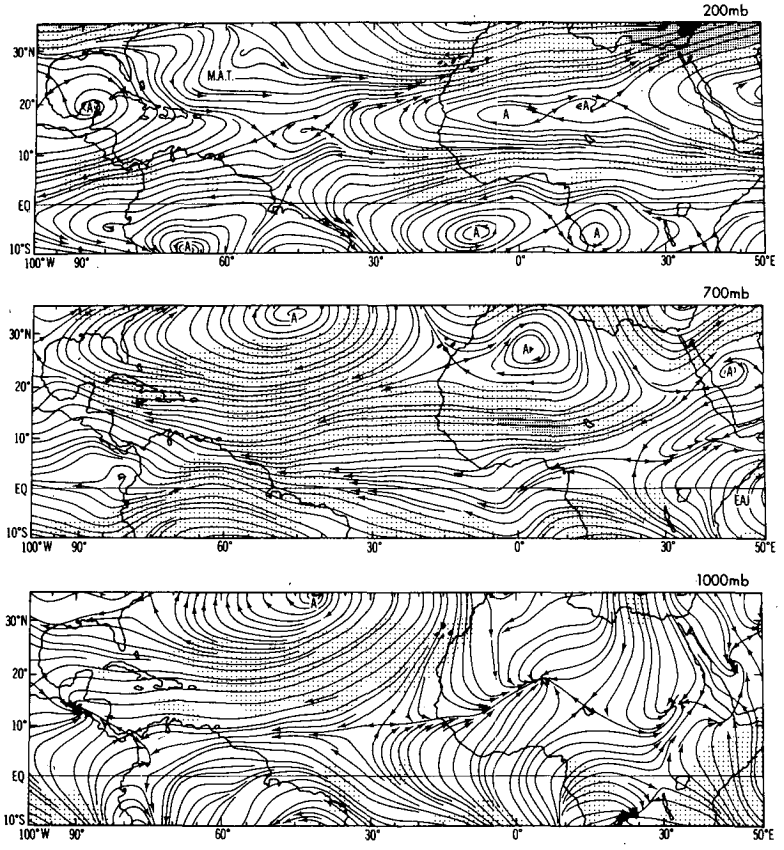

FIG. 6. Phase III mean streamlines and isotachs at 200, 700 and 1000 mb. At 200 mb the light, medium and dark shadings correspond to areas with wind speeds > 10, 20, and 30 m s^{-1}, respectively. At 700 and 1000 mb, light, medium and dark shadings correspond to areas with wind speeds greater than 5, 10, and 15 m s^{-1}, respectively.

trough, and has less of a southwestward extent. There are two major anticyclonic circulation cells, i.e., the mid-Atlantic and north African anticyclones. The trough over Egypt is pronounced. Associated with this trough, air flows clockwise from Europe around the Sahara. To the south of the north-central African anticyclone is the lower-tropospheric easterly jet, which is an important ingredient for generation of African waves on the 3000 km scale. Another outstanding feature is the east African jet (EAJ), located over Madagascar, Kenya and Somalia. The wind speed distribution is in good agreement with Reynolds.

At 1000 mb (bottom of Fig. 6), the confluence line over the Atlantic Ocean is clearly defined at about 10°N. It remains a point of controversy whether this confluent asymptote is a part of the ITCZ (Intertropical Convergence Zone) system or not. Heavy cloudiness and rainfall, which are often ascribed to the ITCZ, are located about 1–4° south of the confluence line (Sadler, 1975; Estoque and Douglas, 1978) (see also lower part of Fig. 10). Another prominent feature in the 1000 mb flow field is the col over the GATE A/B-scale area. The col in the GFDL analysis is located at 11°N and 27.5°W, coinciding with the position of the pressure trough, which is semi-anchored with little seasonal or interannual variation (Sadler, 1975), located at ~10°N over the ocean but at a somewhat higher latitude over land. The placement of this col is in fairly good agreement with the analysis of Burpee and Dugdale (1975) who place the col at about 8°N, 29°W. These are both in good agreement with the 50-year composite streamline map for September compiled by Aspliden *et al.* (1966), which shows the col at ~10°N, 27°W. Reynolds' (1977) analysis for Phase III, however, puts this col about 7° further west. Lastly, the streamline pattern at 1000 mb over northern Africa is very similar to the field of monthly-mean gradient-level wind obtained by Burpee (1972), although his map is for August.

2) RELATIVE VORTICITY

At 200 mb (top of Fig. 7), there are two major axes of positive vorticity, in agreement with the re-

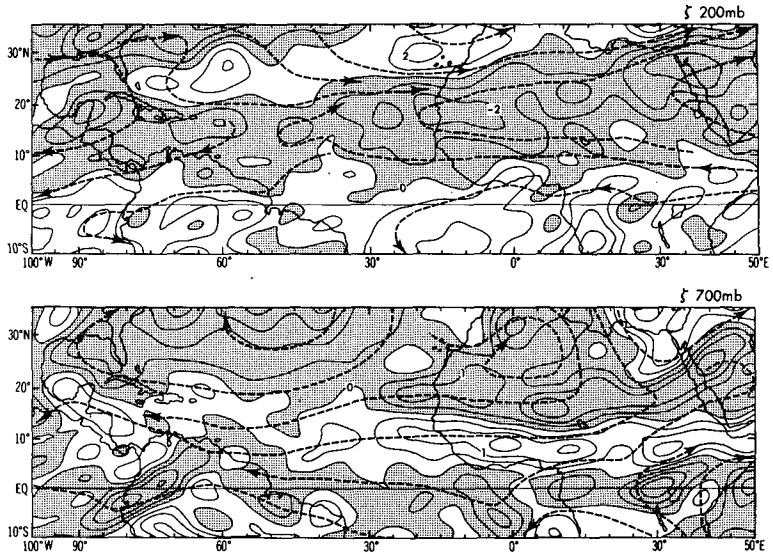

FIG. 7. Phase III mean relative vorticity ζ at 200 mb (upper), and 700 mb (lower). The contour interval is 10^{-5} and 0.5×10^{-5} s^{-1} for 200 and 700 mb, respectively. Negative values are shaded.

sults of Krishnamurti (1971). One is distributed northeast to southwest from the Mediterranean Sea through Morocco to the Bahama Islands, associated with mid-Atlantic trough. The other is located near the equator, south of the upper tropospheric African jet. Over the A/B-array, negative relative vorticity is present at this level in contrast to the positive vorticity at lower levels. This result is in agreement with the results of Thompson *et al.* (1979).

At 700 mb (bottom of Fig. 7), the salient feature is the positive vorticity belt which lies to the south of the Sahara, and extends westward over the Eastern Atlantic. This belt is partly a manifestation of the easterly wave paths, which appear to originate from Nigeria or Cameroon. The positive vorticity east of Sudan is not associated with the African waves, although it appears to be connected with the maximum to the west. The positive vorticity over Saudi Arabia and the Gulf of Aden can be attributed to a semi-permanent trough in that region, on the cyclonic shear side of the EAJ.

3) VERTICAL VELOCITY, $\omega = dp/dt$

Vertical velocity was by far the most difficult field to obtain. One should expect, rightfully, that vertical motions taken directly from the four-dimensional analysis would show an inordinate amount of noise due, in part, to the forcing of wind, temperature, and moisture data onto the model. This does indeed occur both in the daily maps and for the phase III mean (not shown).

Since these vertical motions seemed somewhat unsatisfactory, a special effort was made to try to obtain a less perturbed field. First, a nonlinear normal mode initialization was applied to the results of the static analysis. The method used was that of Machenhauer (1977), the purpose of which is to adjust the analysis so as to control the amplification of the short period (<6 h) gravity waves. The nonlinear normal mode initialization has been known to cause a deterioration in the tropical circulation. However, the extent of the deterioration depends greatly on the period of the waves which are initialized. For this reason, only gravity waves with a period of <6 h were initialized. In this version of the initialization, however, the effect of latent heating is not included, so that the adjustment in the tropics is somewhat lacking. But the overall effect is to smooth the mass and wind fields in a dynamically consistent way, thus achieving our immediate objective. The 700 mb ω-field which results, averaged over phase III, is shown in the upper panel of Fig. 8. Centers of particularly strong upward motion are found over Ethiopa and Uganda (upslope flow over the African highlands), Cameroon (associated with the formation of easterly waves), over Guinea in west Africa (corresponding to the intensifying easterly waves), over Colombia (upslope flow over the northern Andes), and along Latin America (partly a statistical result of the two hurricanes).

Over the A/B-array there is upward motion, albeit weak, consistent with the vertical motion field over the B-array obtained by Reeves *et al.* (1979) and others.

A second step taken in trying to obtain a suitable vertical motion field was to make a 3 h forecast starting from the newly initialized state. There were two

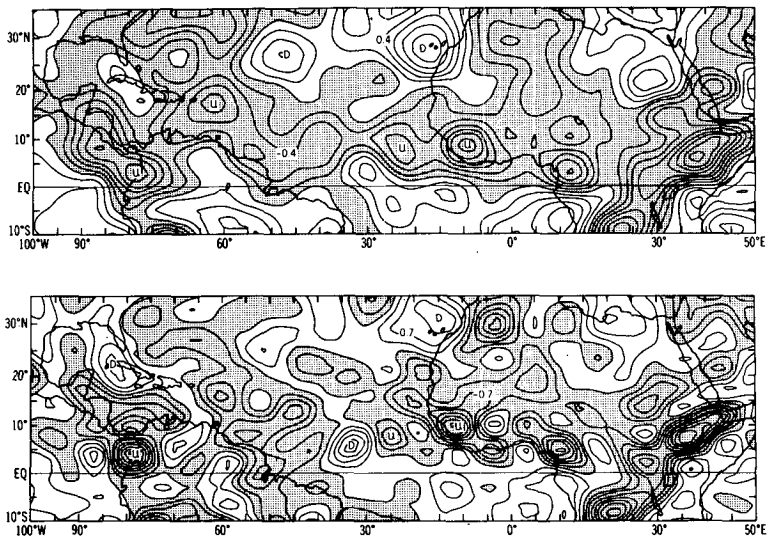

FIG. 8. Phase III mean vertical pressure velocity ω at 700 mb, after nonlinear normal mode initialization (upper) and after a 3 h forecast (lower). The contour interval is 0.2×10^{-3} mb s^{-1} and 0.35 mb s^{-1}, respectively. Negative values (upward motion) are shaded.

principal reasons for doing this. First, the vertical motions obtained from the nonlinear normal mode initialization were quite weak, and it was believed that a short forecast would provide time enough for the various circulations to regain some of their intensity. Second, since latent heating is so important in tropical motions, this would give the model a chance to incorporate its effects. This argument is, of course, based on the premise that the model's parameterization of the latent heating is correct, but this will be discussed at greater length later.

The ω-field derived from these forecasts, averaged over phase III, is shown in the bottom panel of Fig. 8. Overall, the broad pattern is quite similar. The major difference occurs in the degree of smaller-scale variations. Some of this may simply be noise, caused by small imbalances remaining in the initial conditions, which are a reflection of the imbalances set up

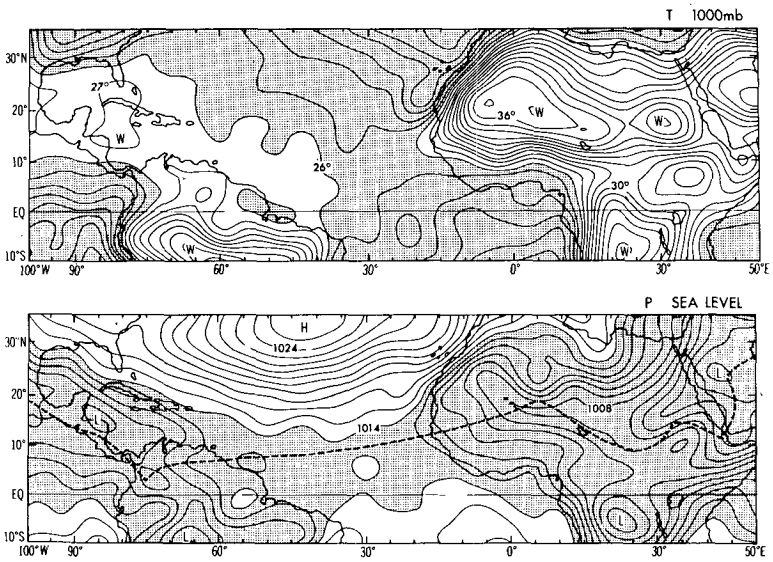

FIG. 9. Phase III mean temperature, T, at 1000 mb (upper). The contour interval is 1°C. Regions with temperature < 26°C are shaded. Phase III mean surface pressure, P_{SL} (lower). The contour interval is 1 mb. Regions with pressure < 1014 mb are shaded. Confluence lines are indicated by dashed lines.

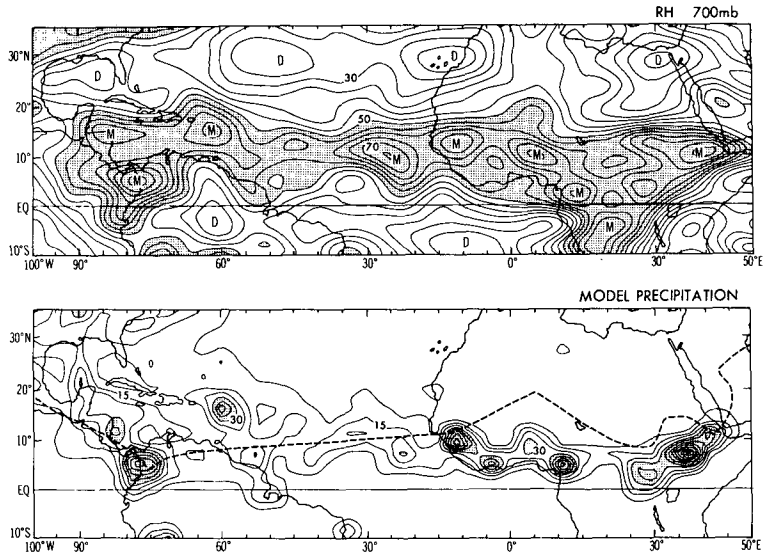

FIG. 10. Phase III mean relative humidity RH at 700 mb (upper). The contour interval is 5%. Regions with humidity > 50% are shaded. Model-generated precipitation (condensation) RC total for Phase III (lower). The contour interval is 7.5 cm. Regions > 30 cm are shaded. Confluence lines are indicated by dashed lines.

when data were being forced on the model during the assimilation. Indeed, these ω-values look remarkably like those obtained directly from the assimilation itself (not shown). However, we believe that this smaller-scale variation is primarily a function of the manner in which the model handles condensation and the concomitant latent heat release. It appears that the simple convective adjustment procedure used here is probably too crude and results in too much "shocking", and this is particularly evident in the tropics, where forcing on the synoptic scale is significantly weaker. A more sophisticated convective parameterization scheme which would reduce this shocking would be more desirable in this regard and is currently being considered.

4) TEMPERATURE T AND SEA LEVEL PRESSURE P_{SL}

The 1000 mb temperature field (upper panel of Fig. 9) is largely a reflection of the intense surface heating over land and surface temperature over sea, although a poleward decreasing tendency is superposed on it. Particularly high temperatures are found over the Sahara desert, equatorial South America, and southern Africa. A warm tongue extends from West Africa into the Atlantic, corresponding to the monsoon trough. The warmer temperatures in the western Atlantic are largely a consequence of warmer sea temperatures. It is generally accepted that the warmth over the Caribbean (27°C) is an important and necessary condition for hurricane genesis.

The surface pressure distribution (lower panel of Fig. 9) is closely related to the surface temperatures. The monsoon trough (Sadler, 1975) starts at 12°N at the coast of West Africa and extends westward at about 8°N.

5) RELATIVE HUMIDITY RH AND PRECIPITATION RC

The moist regions at 700 mb (upper panel of Fig. 10) are mostly confined to the area south of 20°N over both the African continent and the Atlantic Ocean. The highest humidities occur over Nigeria (associated with the formation or development of easterly waves), Colombia (due to the Andes), over the GATE A/B-array (generated by easterly waves), Ethiopia (caused by EAJ), and over the Caribbean (associated with the re-development of the easterly waves).

The general distribution of RH at 700 mb resembles that of the outgoing longwave radiation measured by the NOAA 5 polar orbiting satellite (Winston-see Houghton, 1977) as well as the infrared image brightnesses observed by the geostationary satellite (Murakami, 1979). The primary difference is that the maximum in the satellite data is located over the West African coast (15°W) instead of at 25°W or 10°W, as in Fig. 10.

Precipitation obtained in the four-dimensional analysis is displayed in the bottom of Fig. 10. We want to emphasize here that this is the *model-generated* precipitation and is in no way intended to represent an *analysis* of the phase III precipitation. Furthermore, this precipitation is largely convective in nature and is therefore a product of a convective parameterization. These caveats aside, this does rep-

resent one method, albeit indirect, of obtaining a rough estimate of the distribution of precipitation. It also provides a measure by which to judge the model's ability to handle moisture.

Sadler (1975) stressed that the zone of maximum cloudiness is located to the south of the trough, and the 6-year mean monthly cloudiness for September shows a zonal distribution centered at 6°N. The precipitation shown in Fig. 10 is in good agreement with this distribution. However, Sadler's zone of maximum cloudiness is for all types of clouds, precipitating and non-precipitating, and may give a false impression of the true rainfall distribution. A direct and detailed comparison of the model's rainfall with satellite infrared estimate for the Phase III period does not show such good agreement (see Murakami, 1979). The infrared photograph indicates a zonally oriented area of convective activity, with a maximum over the West African coast and a decrease in activity to the west over the Atlantic, while the precipitation generated by the assimilation model shows two maxima over the same region, and a wavy configuration. Estimates of precipitation derived by Woodley *et al.* (1975, 1980) from satellite infrared measurements also show a maximum centered over the African coast at ~11°N, with decreasing amounts located in a westward-narrowing band centered at 8°N. Our precipitation, while somewhat smoother than the vertical velocity field depicted in Fig. 8, is probably affected by the noise generated. It also suffers from a lack of spatial resolution as well as a rather simple cumulus parameterization.

Other areas with large amounts of precipitation are located over Ethiopia, Cameroon and Colombia. Secondary maxima are found over Uganda, east of the Lesser Antilles (east of the Caribbean), north of Guyana in South America, and over the GATE A/B-array. It is interesting to note that this distribution of rainfall is highly correlated with the humidity distribution shown in Fig. 10. It is perhaps even more interesting to note the excellent correlation of precipitation with the vertical velocity, ω, at 700 mb shown in the lower panel of Fig. 8. This correlation between rainfall and ω is much better at 700 mb than at 850 mb, the reason being unknown. In principle, the precipitation due to cumulus convection is not necessarily correlated with the time-mean large-scale vertical motion, because tropical rain is believed to be caused in large part by transient disturbances in which enhanced cumulus convection is involved. (see Cho and Ogura, 1974). Nevertheless, this result indicates that the relationship between the large-scale stationary component of vertical motion and rainfall does hold, at least in an approximate sense.

In summary, the zone of maximum cloudiness starts at ~8°N over the west coast of Africa and extends westward to South America. The rainfall appears to be caused by disturbances (easterly waves) moving through the monsoon westerlies over West Africa and the easternmost Atlantic into the mid-Atlantic. As the easterly waves propagate westward, their tracks start to deviate northward from the ITCZ in the middle of the Atlantic, say at 40°W, and away from the favorable influences of the large scale flow. It remains a question, then, as to what type of disturbances maintain the ITCZ in the western half of the Atlantic.

b. Meridional sections

Let us turn to meridional sections (i.e., latitude–height distributions) of the various variables during Phase III. The display of each variable consists of three sections corresponding to three longitudinally bounded regions: (A) West Africa (15°W–30°E), (B) central and eastern Atlantic (60–15°W), and (C) West Indies–Caribbean Sea (95–60°W). These regions were chosen based on the characteristics of the easterly waves in each; i.e., formation (A-region), propagation (B-region), and re-development or hurricane genesis (C-region). The selection of regions is very similar to that of Tripoli and Krishnamurti (1975).

A number of studies have been conducted in the past regarding the processes in the A-region, e.g., Carlson (1969), Burpee (1972, 1974); Dean and LaSeur (1974), and Aspliden *et al.* (1976); regarding the processes in the B-region, e.g., Simpson *et al.* (1968) and Frank (1969); and regarding the processes in C-region, e.g., Riehl (1954), Dunn and staff (1963), Yanai (1968) and Gray (1968, 1979).

It is understood from these previous works that the necessary conditions for easterly wave development in the A-region is horizontal shear instability, and that the necessary conditions for tropical cyclone development in the C-region are: conditional gravitational instability, high sea surface temperature, a deep moist layer, a reasonable vertical component of the earth's rotation rate, and small vertical wind shear. Questions still remain as to how much the baroclinic instability contributes to the wave development in the A- and C-regions, and as to how essential condensation is for the easterly wave formation in the A-region, and for the maintenance of the waves in the B-region.

The following series of cross-sections is intended to display more readily the vertical and latitudinal distribution of variables. The parameters displayed are: the stationary and transient components of vorticity, the zonal wind component, the vertical velocity, the humidity, the baroclinic energy conversion, and the barotropic energy conversion.

Before describing the equations of energy, let us introduce the averaging notations. The time average over the Phase III period is denoted by parentheses, and the longitudinal average over the respective do-

mains, i.e., A-, B- and C-regions, is expressed by square brackets. The deviation from the zonal mean is denoted by parentheses with prime. For example, an arbitrary variable x is written by

$$x = [x] + x'. \tag{1}$$

The energetics we are concerned with in this paper are the eddy kinetic energy, $k_E = \frac{1}{2}(u'^2 + v'^2)$, and the eddy available potential energy, $a_E = \frac{1}{2}T'^2/N^2$, where N is a measure of the static stability. The energy equations, which are areally averaged for the respective regions, are written (see for example, Norquist *et al.*, 1977; Smith *et al.*, 1977) symbolically by

$$\frac{\partial K_E}{\partial t} = C(A_E, K_E) + C(K_z, K_E) + B(K_E) - D(K_E) + KP_s, \tag{2}$$

$$\frac{\partial A_E}{\partial t} = C(K_E, A_E) + C(A_z, A_E) + B(A_E) + G(A_E) - D(A_E) + AP_s, \tag{3}$$

where K_E and A_E are the area-averaged k_E and a_E, respectively. C's are the area-averaged conversions kinetic energy, and zonal available potential energy, respectively. C's are the area-averaged conversions of one kind of energy to another. For example, $C(A_E, K_E)$ denotes the conversion from a_E to k_E. $B(K_E)$ is the boundary flux of k_E and ϕ_E (eddy component of geopotential), $B(A_E)$ is the boundary flux of a_E, $D(K_E)$ is the conversion from k_E to subgrid-scale kinetic energy, which represents, in large part, the eventual dissipation of kinetic energy, $G(A_E)$ is the generation of a_E due to diabatic heating, $D(A_E)$ is the conversion from a_E to subgrid-scale available potential energy, which represents, in large part, the dissipation of potential energy, KP_s is the change in k_E due to change in surface pressure, and AP_s is the change in a_E due to change in surface pressure.

The terms for which we have tentative results and which will be displayed here are the baroclinic conversion, $C(A_E, K_E)$, and the barotropic conversion, $C(K_Z, K_E)$. These terms are calculated on pressure surfaces by

$$\overline{C(A_E, K_E)} = -\overline{C(K_E, A_E)} = -\frac{R}{P}\overline{[\omega' T']},$$

$$\overline{C(K_Z, K_E)} = \cos[u'v']\frac{\partial}{a\partial\varphi}\left(\frac{[u]}{\cos\varphi}\right) + [v'^2]\frac{\partial[v]}{a\partial\varphi} + \frac{1}{a}\tan\varphi[v][u'^2] + [\omega' u']\frac{\partial[u]}{\partial p} + [\omega' v']\frac{\partial[v]}{\partial p},$$

where a is the radius of the earth. The velocity and temperature data are taken from the three-hour forecast discussed earlier.

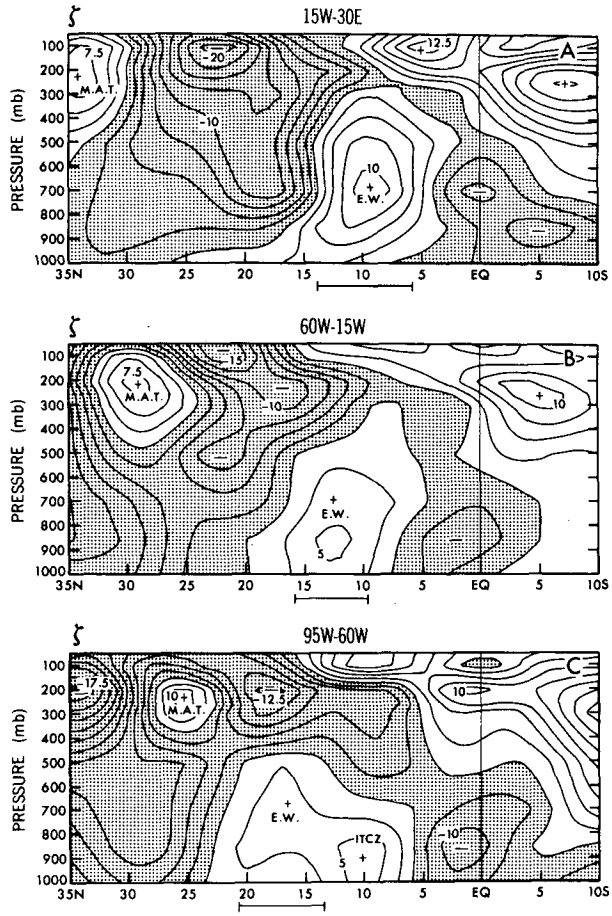

FIG. 11. Meridional cross-sections of zonal and temporal mean of relative vorticity, $[\bar{\zeta}]$, for the A-region (top), B-region (middle), and C-region (bottom). The contour interval is 2.5×10^{-6} s^{-1}. Negative values are shaded.

As mentioned earlier, each of the variables in the cross-sections has been averaged over the Phase III period and over the longitudes of the respective domain. For convenience, the central positions of easterly waves (EW), the mid-Atlantic trough (MAT), and the ITCZ are noted for each of the regions. The latitudinal extent of easterly wave activity is also indicated by a short horizontal bar at the bottom of each panel.

1) RELATIVE VORTICITY $[\bar{\zeta}]$ (FIG. 11)

The positions of EW are taken from Fig. 12. The positive vorticity associated with the MAT and the path of the EW is very evident in all three regions. These two features, as well as the ITCZ, are the most outstanding tropospheric phenomena observed in the whole GATE area. The separate vorticity maximum at 10°N in the C-region is primarily a reflection of

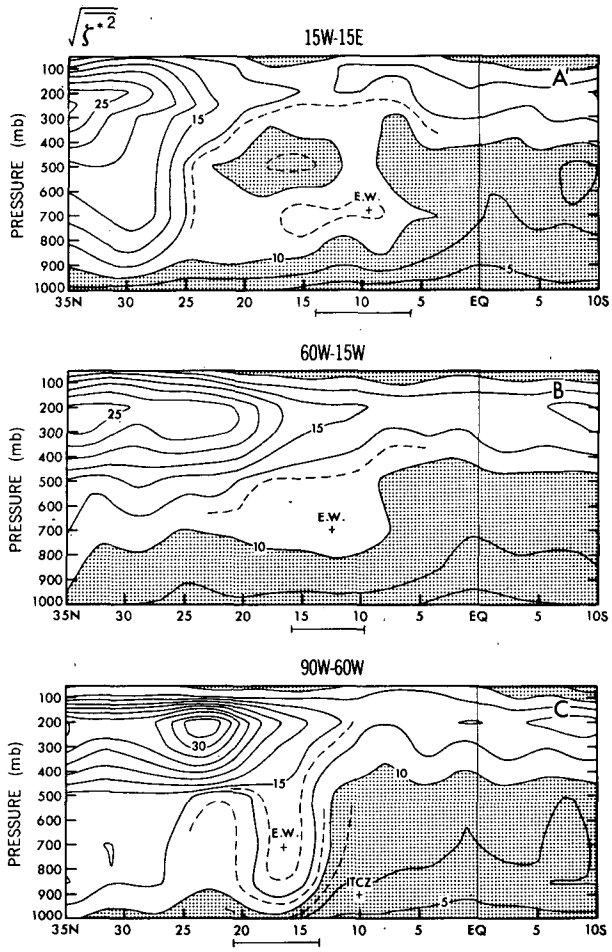

FIG. 12. As in Fig. 11, but for the root mean square transient component of relative vorticity, $([\zeta^{*2}])^{1/2}$. The contour interval is 2.5×10^{-6} s^{-1}. Values $< 10^{-5}$ s^{-1} are shaded.

a renewed ITCZ west of 75°W, since a distinct axis of convergence is difficult to identify west of ~45°W (see Fig. 6).

2) Root-mean-square transient component of vorticity $([\overline{\zeta^{*2}}])^{1/2}$ (Fig. 12)

The relative vorticity is divided into two components,

$$\zeta = \bar{\zeta} + \zeta^*,$$

where $\bar{\zeta}$ is the vorticity averaged over the Phase III period, shown in Fig. 11, and ζ^* is the rest of the vorticity, i.e., the transient component. Fig. 12 is the rms transient component of vorticity, which may indicate the intensity of easterly wave. For convenience of calculation the first domain in this particular figure was taken from 15°E to 15°W, which is different from the A-region in the rest of cross-sections. The maxima at 700 mb are marked by crosses and EW, indicating the central position of easterly waves.

3) Zonal wind component $[\bar{u}]$ (Fig. 13)

In the A-region, the upper tropospheric easterly jet is located at the 200–100 mb level and 5–10°N, and the lower-level easterly jet is located at the 650 mb level at ~15°N. The upper tropospheric westerlies are found at the 200 mb level around 30°N and are associated with the MAT.

The path of the easterly waves, as determined by the maximum in vorticity, lies precisely where the horizontal wind shear is largest. In the B- and C-regions, the horizontal shear is not as strong. A striking feature in the C-region is that there is no significant vertical wind shear at the latitude of the EW. Note also that the position of the MAT is shifted southward compared with that of other regions.

4) Vertical velocity $[\bar{\omega}]$ (Fig. 14)

The vertical velocities shown in Fig. 14 are those derived from the four-dimensional assimilation and so include the effect of latent heating. The latitudes

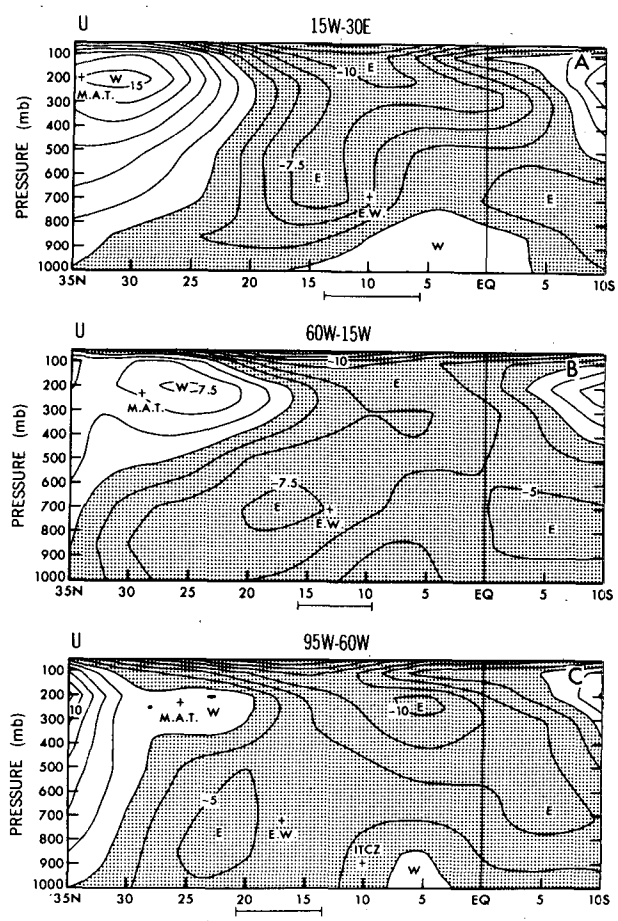

FIG. 13. As in Fig. 11, but for zonal wind component $[\bar{u}]$. The contour interval is 0.25 m s^{-1}. The centers of the westerlies and easterlies are marked by W and E, respectively. Negative areas (easterlies) are shaded.

of the EW correspond to updraft areas in all three regions. In the B-region, there is a somewhat questionable downdraft south of 8°N, evident in Fig. 8. This to a large extent is the reason why the maximum upward velocity is located at ~16°N. Observations suggest that it should be further south. In the C-region, the hurricane formation region corresponds to a region of strong ascent.

5) RELATIVE HUMIDITY [$\overline{RH}$] (FIG. 15)

The regions of high relative humidity correspond quite closely to the regions of upward motion in Fig. 14, as might be expected. The EW correspond to areas of high humidity in all three regions. Humidities are particularly high in the C-region.

6) THE BAROTROPIC ENERGY CONVERSION $\overline{C(K_Z, K_E)}$ (FIG. 16)

The barotropic conversion from K_Z to K_E shows positive values in the vicinity of EW for both the A- and B-regions. This value is particularly large in the B-region. Norquist *et al.* (1977) found that $\overline{C(K_Z, K_E)}$ is larger over the ocean (30–15°W) than over land (15°W–10°E). Our result tends to agree with theirs, at least along the easterly wave path, though the domain separation is defined somewhat differently. Tripoli and Krishnamurti (1975) mentioned that the C-region is barotropically stable at 850 mb level. This feature is also seen in our case; at 850 mb, $\overline{C(K_Z, K_E)}$ is negative. A difference from Norquist *et al.* is that the magnitude of our barotropic conversion is much smaller than that of the baroclinic conversion in general. We believe this to be due to the method employed by Norquist *et al.* (and also Edmon and Vincent, 1977). Their calculations are based on a coordinate system moving with the wave, in contrast to the Eulerian method employed here, and the barotropic conversion may indeed be much more significant within the wave itself.

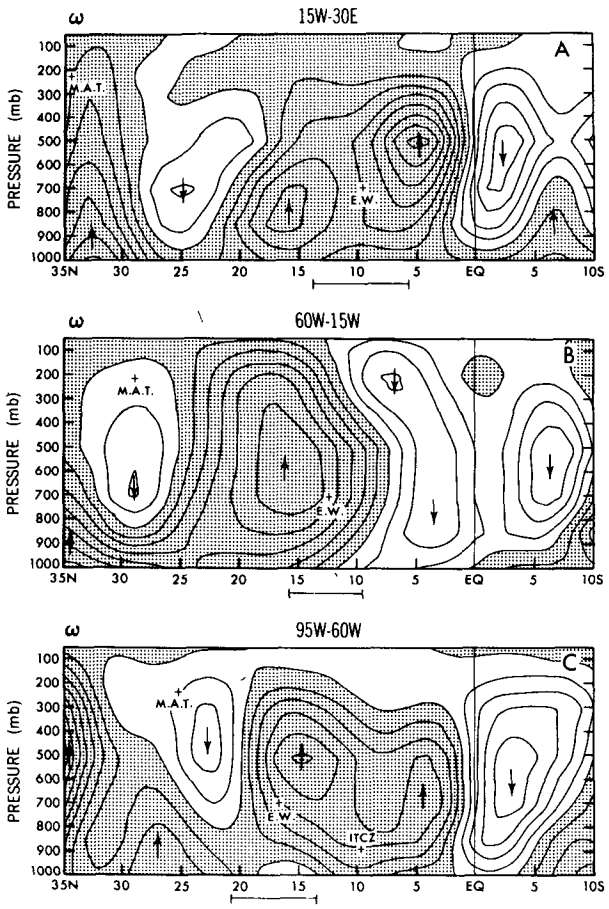

FIG. 14. As in Fig. 11, but for vertical pressure velocity [$\bar{\omega}$]. The contour interval is 10^{-4} mb s^{-1}. Negative values (upward motion) are shaded. Arrows indicate the updraft and downdraft.

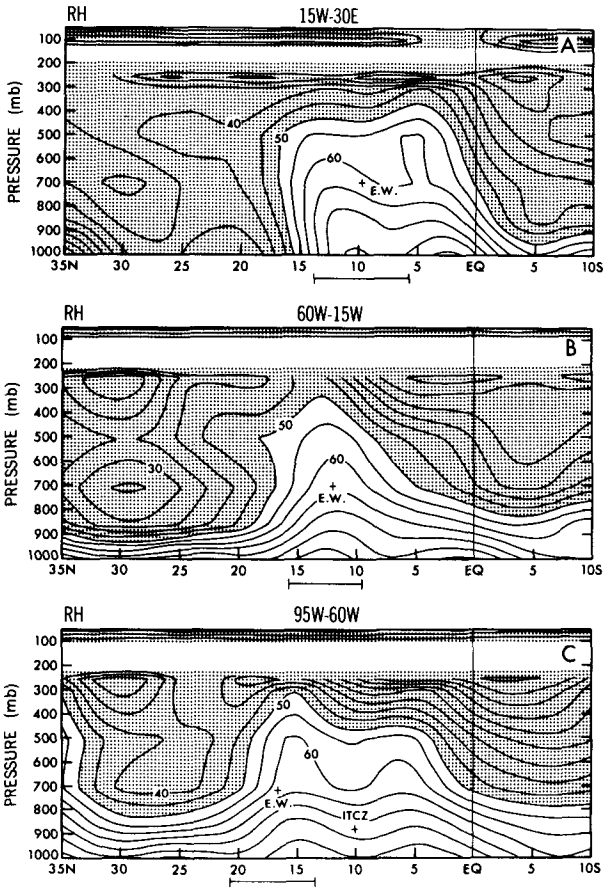

FIG. 15. As in Fig. 11, but for relative humidity RH. The contour interval is 5%. Regions with humidity < 50% are shaded.

7) THE BAROCLINIC ENERGY CONVERSION $\overline{C(A_E, K_E)}$ (FIG. 17)

Manabe *et al.* (1970) pointed out, based on a GCM study, that the baroclinic conversion is the

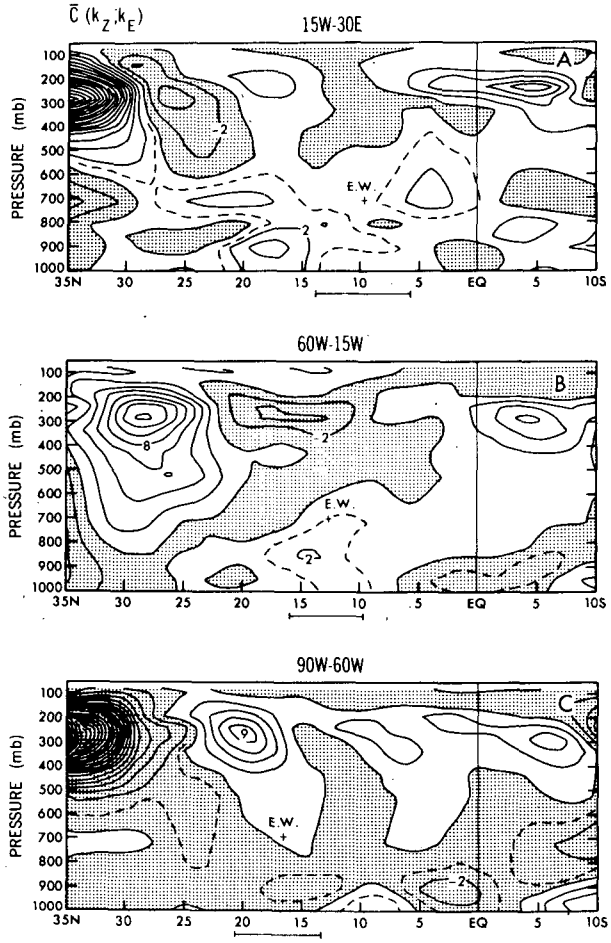

FIG. 16. As in Fig. 11, but for barotropic energy conversion $C(K_Z, K_E)$. The contour interval is 1.0×10^{-4} W (kg)$^{-1}$. Negative areas ($K_E \rightarrow K_Z$) are shaded.

major source for K_E in the tropics. $\overline{C(A_E, K_E)}$ in Fig. 17 are indeed dominated by positive conversion for all three regions below about the 200 mb level. Maxima tend to be located just over the equator and at ~15°N, which is consistent with Manabe *et al.* (1970, 1974). Another pronounced feature in the tropics is that the upper tropospheric maxima of $\overline{C(A_E, K_E)}$ is located at the 200 mb level, which is substantially higher than in the extratropics. This was noted earlier by Kung (1965), Nitta (1979), Wallace (1971) and Kung and Meritt (1974), though the maxima were located nearer 300 mb in these studies. However, the part of $C(A_E, K_E)$ that contributes to the easterly wave development or decay lies at the lower levels.

Along the path of the easterly waves, $C(A_E, K_E)$ is largest in the C-region, particularly to the east of the Caribbean Sea, due to the increase in sea surface temperature over which the easterly waves are propagating. In the C-region, the re-development of easterly waves to the east of Puerto Rico appears to be largely due to the baroclinic conversion despite the smallness of the vertical wind shear. In region A, the baroclinic conversion is actually slightly negative at the level and latitude of the easterly waves, becoming even more negative below 700 mb and to the south. This is in good agreement with the findings of Norquist *et al.* (1977), despite their entirely different approach.

A summary of the barotropic and baroclinic energy conversions is given in Table 1. The terms were integrated over the previously mentioned longitudinal spans as well as vertically from 125 to 1000 mb. For the A- and B-regions, the integrations were performed over the latitudinal span 0–20°N, while that over the C-region was taken from 5 to 25°N. The units are W m^2. In each of the areas, the baroclinic conversion is at least several times larger than the barotropic conversion but, again, this may not hold true within the waves themselves. Both of the conversions are largest in the A-region, as one might expect since this is the region of easterly wave formation.

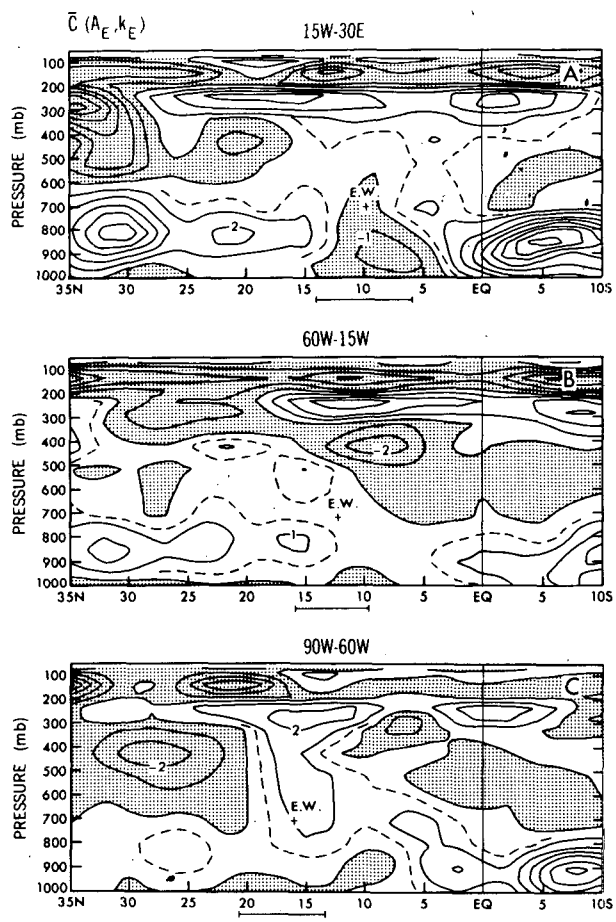

FIG. 17. As in Fig. 11, but for baroclinic energy conversion $C(A_E, K_E)$. The contour interval is 1.0×10^{-4} W kg^{-1}. Negative areas ($K_E \rightarrow A_E$) are shaded.

TABLE 1. Summary of barotropic and baroclinic energy conversions.

	Region		
	A	B	C
$C(A_E, K_E)$	0.45	0.19	0.31
$C(K_Z, K_E)$	0.08	−0.01	0.04

8) REMARKS

The mechanism of wave formation over Africa has been investigated and discussed by several authors (e.g., Rennick, 1976; Simmons, 1979; Mass, 1979). Using the GATE data, Norquist *et al.* (1977) and Thompson *et al.* (1979) have studied this problem through an estimate of the energy budget. Our study seems to suggest that while baroclinic conversion is larger on average, the contribution to wave development or formation by barotropic conversion may be significant. However, the effect of latent heat release may be quite important, particularly over the African continent, although the initial trigger might still be the barotropic instability. A more direct answer may be provided by prediction experiments such as those of Pedgley and Krishnamurti (1976), Krishnamurti *et al.* (1979), and Lyne *et al.* (1976), but the choice of convective parameterization may be all-important to determine the role of latent heat release.

Concerning the hurricane genesis in C-region, an approach along the line of Kurihara and Tuleya (1981) and Jones (1980) is a promising way to understand the energetics. In our opinion, the analyzed data can be utilized by the nested grid method for the prediction experiment of hurricanes.

4. Some transient phenomena

The structure and properties of African easterly waves have been extensively studied by Burpee (1975), Reed *et al.* (1977), Thompson *et al.* (1979) and others, using the compositing technique of Reed and Recker (1971). Here we attempt to investigate another aspect of these disturbances, i.e., their propagation characteristics and associated condensation.

a. Hovmöller diagram of easterly waves

The time-latitude charts (Hovmöller diagrams) shown in Figs. 19 and 20 are based on relative vorticity at the 700 mb level. The thick dashed lines in Fig. 18 are the lines along which the Hovmöller diagrams were taken. Note that two lines are shown over eastern Africa east of 15°E. Path a approximately follows the low level (i.e., 700–850 mb) flow, while path b follows roughly the 500 mb flow. We present only the results from path a, since it more nearly reflects the level at which the processes of interest are occurring, although neither path displays any clear propagation east of 20°E.

Also shown in Fig. 18 are the paths of the cyclonic vortices (easterly waves) and hurricanes based on the atlas compiled by Sadler and Oda (1978). (See also Hope, 1975.) The cyclone tracks obtained by Dean and LaSeur (1974) are shown by the shaded swath over central Africa.

The Hovmöller diagram for vorticity at the 700 mb level (Fig. 19) reveals a very systematic movement of the easterly waves from east to west, a characteristic which has long been recognized, for example, by Chang (1970), who used cloud clusters to trade their motions, and interpreted as a Rossby wave by Rosenthal (1960). We have adopted the S-O system for numbering the vortices and plotted this number beside the corresponding track.

Fig. 20 depicts the tracks of the individual easterly waves, as analyzed by Sadler-Oda and by the GFDL analysis system. Sadler and Oda's tracks were derived from surface charts, while those from the GFDL analysis were taken from the 700 mb charts. The agreement between the two analyses is ex-

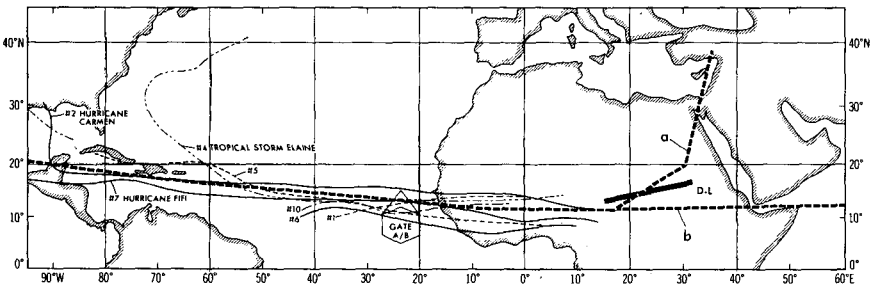

FIG. 18. The solid dashed line is the line along which Hovmöller diagrams in Figs. 20 and 21 were constructed. The line follows the mean path of the tropical low-level vortices (easterly waves) and Atlantic hurricane tracks in 1974. The numbers identifying each track are taken from Sadler and Oda. The shaded swath labeled D-L indicates the region traversed by easterly waves in August, 1970, as compiled by Dean and LaSeur (1974). The GATE A/B-array is shown by the hexagon at 23°W, 8°N.

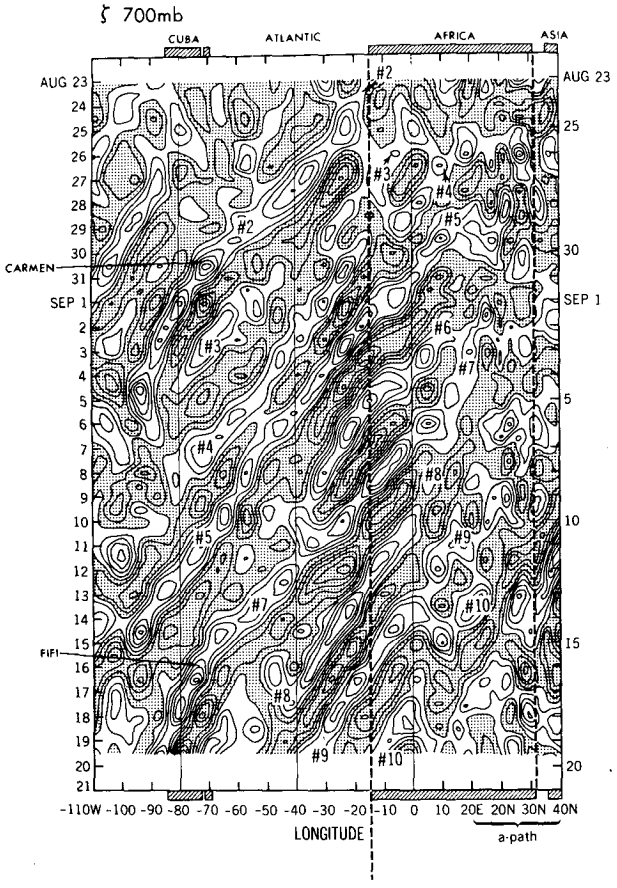

FIG. 19. Hovmöller diagram of relative vorticity ζ at 700 mb along the path a in Fig. 18. To the left of 15°W, the abscissa is longitude and to the right it is latitude. The dashed lines at 18°W and 30°N indicate the African coastlines. The contour interval is 0.5 10^{-5} s^{-1}. Regions of negative vorticity are shaded. Sadler's and Oda's numbering system is adopted in labeling the waves.

tremely good, and does not show a single significant discrepancy with regard to position or displacement.

Fig. 20 also plots precipitation estimates made from infrared imagery of the Geosynchronous Meteorological Satellite (SMS-1) (GATE Data Catalog, No. 5. 89.02.102). The agreement between the precipitation maxima and the tracks of waves seems to be good, indicating that the four-dimensional analysis has successfully reproduced all easterly waves, at least qualitatively.

Thus the accuracy of the Hovmöller diagram is supported by two independent studies. Let us now turn back to the formation region of the disturbances. This region appears to be located between longitudes 10 and 30°E, i.e., Nigeria, Chad, and/or Sudan. This problem of locating the genesis region has been actively discussed. For example, Dean and LaSeur (1974) noted that the synoptic-scale variations typically form in the eastern portions of tropical Africa near Sudan (13–18°N). If latent heating is assumed to be an important source of energy for the developing wave, then convective outbreaks could play a role in this region. Aspliden *et al.* (1976), in a study of "African disturbance lines," suggested that the convection-inducing effect of terrain could be important in the Agadez region of Nigeria.

A significant question is whether positive vorticity has been introduced prior to the actual formation of the eddy circulation. Fig. 20 may not be conclusive in this regard, but we can say that the Hovmöller diagram along path a provides a somewhat more continuous pattern of vorticity propagation than does path b, the possible implication being that the initial "seed" for easterly wave formation may come from an area to the north rather than the east.

Figs. 19 and 20 are also informative with regard to the intensities of the easterly waves. In each case, the wave appears to reach a maximum intensity as it passes the African coast, and then decays as it moves out into the Atlantic. Some of the waves subsequently reintensify as they move into the Carib-

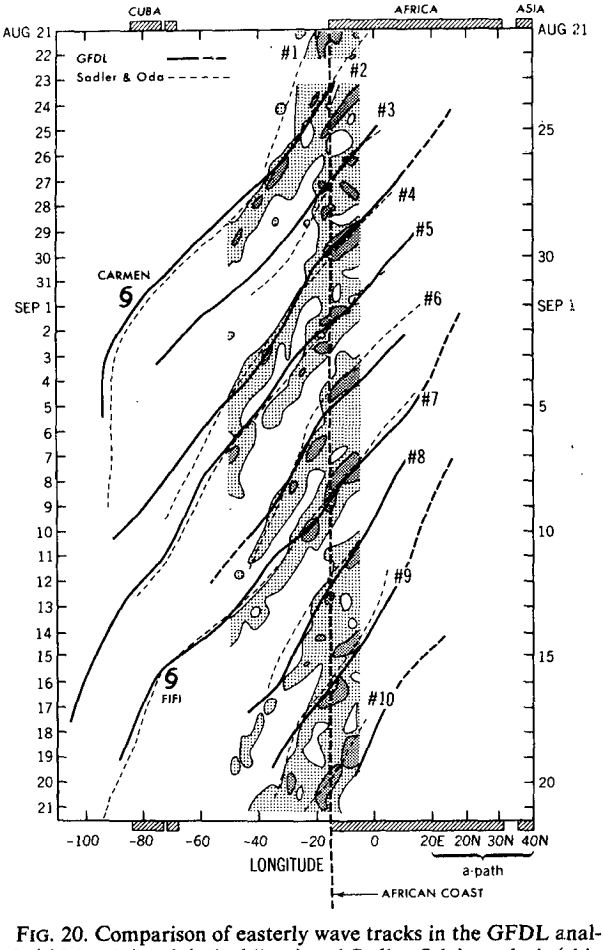

FIG. 20. Comparison of easterly wave tracks in the GFDL analysis (thick solid and dashed lines) and Sadler-Oda's analysis (thin dashed lines). Satellite estimates of precipitation are also shown for the region near the west African coast. Precipitation rates in excess of 0 and 6 mm $(6\ h)^{-1}$ are lightly and heavily shaded, respectively.

bean. During Phase III, easterly wave 2 became Hurricane Carmen; 4 was transformed to Tropical Depression Elaine but moved off to the north; 5 maintained itself as a wave and continued to propagate westward; and 7 developed to Hurricane Fifi.

b. Condensation

A comparison is made of the precipitation rate derived by the four-dimensional analysis and that estimated from the infrared imagery taken by the SMS-1 satellite (Woodley *et al.*, 1975; 1980). Although measurements were made over the GATE A/B-scale area, this is the only data set available which provides estimates of precipitation over the entire ocean. Its accuracy has been checked by ground truth measurements and also by radar estimates (Griffith, *et al.*, 1978; Stout *et al.*, 1979; Hudlow and Patterson, 1979).

Figure 21 is the 6-hourly rate of precipitation averaged over five gridpoints located in the A/B hexagonal-array in Fig. 18, compared to the satellite IR estimates. The agreement is not entirely satisfactory, but a fair degree of correlation may be seen. One can immediately see that the satellite-derived precipitation rates are both shorter-lived and more intense, suggestive of more organized convection. In contrast, the GFDL-analyzed precipitation is almost continuous, although peaks are periodically superposed. We believe this "smearing" of precipitation in time is due to excessive gravity-wave activity generated by the four-dimensional assimilation process.

The high degree of correlation between precipitation and easterly wave passage would seem to indicate that these waves play a dominant role in the production of rainfall, although it is the mesoscale processes such as squall lines which are generally believed to be responsible for the majority of the precipitation. This conclusion is consistent with Murakami's (1979) findings that the largest portion of the transient component in the infrared variations can be accounted for by the westward-moving wave with a period of 4–5 days. Conversely, one can say that the easterly waves are accompanied by condensation and the concomitant release of latent heat.

It has been suggested that this latent heat release may provide a kinetic energy source for the easterly waves. For example, Yamasaki (1969, 1971) and Holton (1970, 1971) noted that easterly waves are "forced Rossby waves." Hayashi (1974) demonstrated that a GCM could produce easterly waves of wavenumber 10 with a period of 5 days, and that these waves are accompanied by precipitation. Yet Pedgley and Krishnamurti (1976) mentioned, based on a prognostic approach with a dry quasi-geostrophic model, that the combined instability of the horizontal and vertical shears in the zonal flow could serve as a sufficient source of eddy kinetic energy through barotropic conversion.

The correlation coefficient between the two sets of precipitation measurements in Fig. 21 is 0.31, and the rms error is 10.5 mm day^{-1}. This result is consistent with the result of Lord (1980) who found the correlation coefficient between the observed rainfall

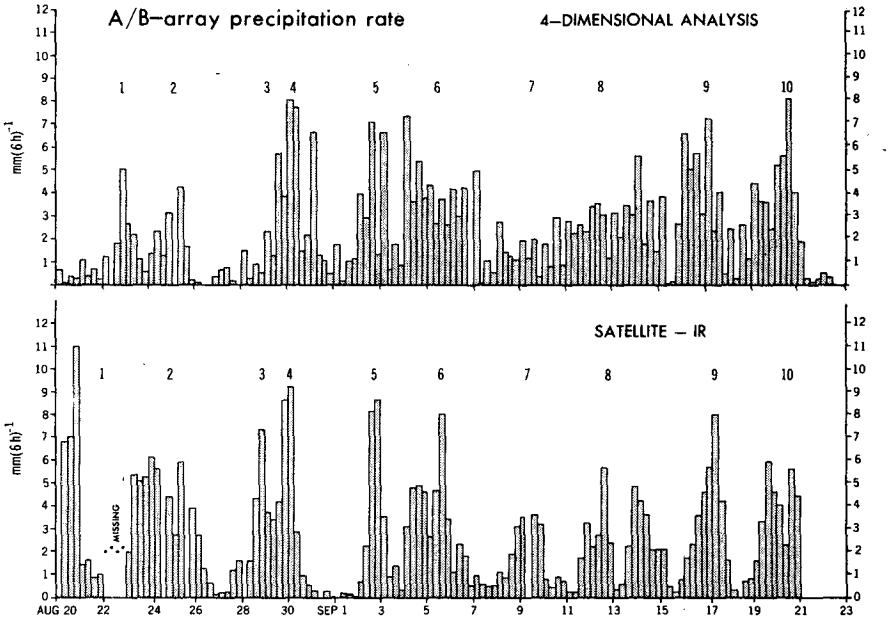

FIG. 21. Time series of 6-hourly precipitation rates over the A/B-array derived by the four-dimensional analysis and from satellite estimates. The passage of easterly waves is indicated, following the numbering system of Sadler and Oda.

and that calculated by the convective adjustment method (75% saturation) to be 0.43. On the other hand, Krishnamurti *et al.* (1980) obtained quite different results. They calculated rainfall utilizing a "hard" convective adjustment (their terminology) and found an rms error of 288 mm day^{-1}, which is 20 times larger than that of the present study. We are unable to explain this discrepancy; it could be due to different adjustment procedures or the extrapolation of the one-step condensation rate to 24 h in their calculation. (Note that the verification domain in this paper is the A/B-array, whereas the studies of Lord and Krishnamurti *et al.* verified over the B-array). Importantly, however, both studies concluded that more accurate results were obtained when the Arakawa-Schubert or Kuo's new methods were used to calculate rainfall amounts.

Our results do leave much room for improvement. Changes in the analysis system which may lead to such improvement include 1) the use of a better parameterization of cumulus convection, 2) the inclusion of diurnal variability with cloud–radiation interaction (Orlanski and Polinsky, 1977; Gray and Jacobsen, 1977; Cox and Griffith, 1979; McGarry and Reed, 1978; Murakami, 1979), and 3) increased suppression of gravity waves. In particular, the convective adjustment technique is believed responsible for the locally concentrated geographic distribution of rainfall (see Fig. 10), in contrast to the rather smoothly distributed precipitation as derived from the satellite measurements.

5. Conclusions and remarks

1) The quality of the revised 1978–79 four-dimensional analysis system has been appreciably improved compared with that of the 1974 version described in Part I, due in part to the addition of supplementary GATE data available in a delayed mode. The spectral GCM with R30L9 resolution employed in the dynamical data assimilation can barely resolve organized waves in the tropics.

2) The tropical wind analysis for the GATE A-scale area is comparable in quality to hand analyses. African and Atlantic low-level cyclones were properly reproduced in the four-dimensional analysis, at least with respect to their positions and displacement.

3) Using the analysis results for the 20-day period of GATE Phase III, a time-averaged state of the tropical atmosphere over the GATE A-scale area was calculated from the mass, wind, thermal and moisture fields, and also for precipitation as revealed in the model analysis. The GATE A-scale area was divided into three regions, i.e., the African continent, Atlantic Ocean and Caribbean Sea, corresponding to various stages in the evolution of the easterly waves, i.e., formation, propagation, and either decay or the re-development of the disturbances (hurricane genesis), respectively. The basic meteorological conditions and the baroclinic and barotropic energy conversions have been investigated for these three regions, and a reasonable, consistent picture for the easterly wave processes has been obtained.

4) The analysis scheme was designed to minimize the model's bias and any excessive model influence. Yet, in the tropics, the analyzed patterns of condensation, vertical velocity and humidity are inevitably inter-related. Even the distributions of vorticity and pressure are, to some extent, influenced by the model's condensation.

5) The easterly waves were investigated in terms of their westward propagation and associated precipitation. The model's precipitation was compared to the satellite estimates over the GATE A/B-array with a fair degree of correspondence (correlation coefficient of 0.31).

Further improvements in this area of research would include: 1) a method of maintaining a greater degree of dynamical consistency between wind and mass fields; 2) a revised cumulus convection parameterization; 3) cloud-radiation interaction; 4) revised treatment of the planetary boundary-layer and soil moisture; 5) inclusion of diurnal variability; and 6) an increase in the spatial resolution of the GCM.

Acknowledgments. The authors are most grateful to Dr. J. Smagorinsky for his continuing support of GATE research, to Dr. D. Sargent and the GATE office for their work in making the data available, to Professor T. N. Krishnamurti for supplying the streamline program, and to Professors J. Sadler and G. Dean for permission to reproduce the maps in this paper. We would also like to thank Dr. J. Fein, Dr. Y. Kurihara, and Professor R. J. Reed for their helpful comments and suggestions, and our colleagues, Mr. T. Jobson, Mr. D. Lee, and Mr. T. Terpstra for their contributions.

The authors also express their thanks to P. G. Tunison and W. H. Ellis for drafting the figures, to J. N. Conner for the photographic work, and to B. M. Williams for typing the manuscript.

REFERENCES

Alaka, M. A., and R. C. Elvander, 1972: Optimum interpolation from observations of mixed quality. *Mon. Wea. Rev.*, **100**, 612–617.

Aspliden, C. I., G. A. Dean and H. Landers, 1966: Satellite study, tropical North Atlantic, 1963, Part I. Res. Rep. 66-2, Dept. Meteor., Florida State University, Tallahassee, 72 pp.

——, Y. Tourre and J. B. Sabine, 1976: Some climatological aspects of West African disturbance lines during GATE. *Mon. Wea. Rev.*, **104**, 1029–1035.

Burpee, R. W., 1972: The origin and structure of easterly waves in the lower troposphere of North Africa. *J. Atmos. Sci.*, **29**, 77–90.

——, 1974: Characteristics of North African easterly waves during the summers of 1968 and 1969. *J. Atmos. Sci.*, **31**, 1556–1570.

——, 1975: Some features of synoptic-scale waves based on compositing analysis of GATE data. *Mon. Wea. Rev.*, **103,** 921–975.

——, and G. Dugdale, 1975: Field phase report of the GARP Atlantic Tropical Experiment. WMO, pp. 2-1 to 2-42.

Carlson, T. N., 1969: Some remarks on African disturbances and their progress over the tropical Atlantic. *Mon. Wea. Rev.*, **91,** 716–726.

Chang, C-P., 1970: Westward propagating cloud patterns in the tropical Pacific as seen from time-composite satellite photograph. *J. Atmos. Sci.*, **27,** 133–138.

Cho, H-R., and Y. Ogura, 1974: A relationship between cloud activity and the low-level convergence as observed in Reed-Recker's composite easterly waves. *J. Atmos. Sci.*, **31,** 2058–2065.

Cox, S. K., and K. T. Griffith, 1979: Estimates of radiative divergence during Phase III of the GARP Atlantic Tropical Experiment: Part II. Analysis of Phase III results. *J. Atmos. Sci.*, **36,** 586–601.

Dean, G. A., and N. E. LaSeur, 1974: The mean structure and its synoptic-scale variation of the African troposphere. *Preprints Int. Tropical Meteorology Meeting*, Nairobi, Amer. Meteor. Soc., pp. 224–228.

——, and C. Smith, 1977: A study of synoptic and mesoscale interaction over the GATE ship network: 4-5-6 September 1974. NCAR Tech. Note, NCAR/TN-122-STR, 95 pp.

Dunn, G. E., and Staff, 1963: The hurricane season of 1962. *Mon. Wea. Rev.*, **91,** 199–207.

Edmon, H. J., Jr., and D. G. Vincent, 1979: Large-scale atmospheric conditions during the intensification of Hurricane Carmen (1974). II. Diabatic heating rates and energy budget. *Mon. Wea. Rev.*, **107,** 295–313.

Estoque, M. A., and M. Douglas, 1978: Structure of the intertropical convergence zone over the GATE area. *Tellus*, **30,** 55–61.

Frank, N. L., 1969: The "inverted-v" cloud pattern—An easterly wave? *Mon. Wea. Rev.*, **97,** 130–140.

Gandin, L. S., 1963: *Objective Analysis of Meteorological Fields.* Gidrometeor. Izdatel, Leningrad (Israel Program for Scientific Translations, 1968, 242 pp.).

Gordon, C. T., L. Umscheid and K. Miyakoda, 1972: Simulation experiments for determining wind data requirements in the tropics. *J. Atmos. Sci.*, **29,** 1064–1075.

——, and W. Stern, 1974: Spectral modelling at GFDL. *The GARP Programme on Numerical Experimentation. Rep. Int. Symp. on Spectral Methods in Numerical Weather Prediction for GARP.* Copenhagen, WMO, 46–82. [WGNE, Research Coordinator for Numerical Methods, Canadian Meteorological Centre, West Isle Office Tower, Trans-Canada Highway, Dorval, Quebec.]

Gray, W. M., 1968: Global view of the origin of tropical disturbances and storms. *Mon. Wea. Rev.*, **96,** 669–700.

——, 1979: Hurricanes: their formation, structure and likely role in the tropical circulation. *Meteorology over the Tropical Oceans, Quart. J. Roy. Meteor. Soc.*, Suppl., **105,** 155–218.

——, and R. W. Jacobson, 1977: Diurnal variation of deep cumulus convection. *Mon. Wea. Rev.*, **105,** 1171–1188.

Griffith, C. G., W. L. Woodley, P. G. Grube, D. W. Martin, J. Stout and D. N. Sikdar, 1978: Rain estimation from geosynchronous satellite imagery—Visible and infrared studies. *Mon. Wea. Rev.*, **106,** 1153–1171.

Hayashi, Y., 1974: Spectral analysis of tropical disturbances appearing in a GFDL general circulation model. *J. Atmos. Sci.*, **31,** 180–218.

Holton, J. R., 1970: A note on forced equatorial waves. *Mon. Wea. Rev.*, **98,** 614–615.

——, 1971: A diagnostic model for equatorial wave disturbances: The role of vertical shear of the mean zonal wind. *J. Atmos. Sci.*, **29,** 55–64.

Hope, J. R., 1975: Atlantic Hurricane season of 1974. *Mon. Wea. Rev.*, **103,** 285–293.

Houghton, D., 1977: Summary for ITCZ. Rep. U.S. GATE Central Program Workshop, NCAR, 19–37.

Hudlow, M. D., and V. L. Patterson, 1979: *GATE Radar Rainfall Atlas.* NOAA Special Report, Dept. of Commerce, 155 pp. [Superintendent of Documents, U.S. Government Printing Office, Washington, DC 20402].

Jones, D. E., 1976: The United Kingdom Meteorological Office objective analysis scheme for GATE. *Meteor. Mag.*, **105,** 249–260.

Jones, R. E., 1980: A three-dimensional tropical cyclone model with release of latent heat by the resolvable scales. *J. Atmos. Sci.*, **37,** 930–938.

Krishnamurti, T. N., 1971: Observational study of the tropical upper troposphere motion field during the Northern Hemisphere summer. *J. Appl. Meteor.*, **10,** 1066–1096.

Krishnamurti, T. N., H. L. Pan, C. B. Chang, J. Ploshay and A. W. Oodally, 1979: Numerical weather prediction for GATE. *Quart. J. Roy. Meteor. Soc.*, **105,** 979–1010.

——, Y. Ramanathan, H-L. Pan, R. J. Pasch and J. Molinari, 1980: Cumulus parameterization and rainfall rates. I. *Mon. Wea. Rev.*, **108,** 465–472.

Kung, E. C., 1975: Balance of kinetic energy in the tropical circulation over the western Pacific. *Quart. J. Roy. Meteor. Soc.*, **101,** 293–312.

——, and L. P. Merritt, 1974: Kinetic energy sources in large-scale tropical disturbances over the Marshall Island area. *Mon. Wea. Rev.*, **102,** 489–502.

Kurihara, Y., and R. Tuleya, 1981: A numerical simulation study on the genesis of a tropical storm. *Mon. Wea. Rev.*, **109,** 1629–1653.

Lord, S., 1980: Verification of cumulus parameterizations using GATE data. *Proc. Seminar on the Impact of GATE on Large-Scale Numerical Modelling of the Atmosphere and Ocean*, Woods Hole, 182–191. [U.S. Committee for the Global Atmospheric Research Program, 2101 Constitution Ave., Washington, DC 20418].

Lyne, W. H., P. R. Rowntree, C. Temperton and J. Walker, 1976: Numerical modeling using GATE data. *Meteor. Mag.*, **105,** 261–271.

McGarry, M. M., and R. J. Reed, Jr., 1978: Diurnal variations in convective activity and precipitation during Phases III and II of GATE. *Mon. Wea. Rev.*, **106,** 101–113.

Machenhauer, B., 1977: On the dynamics of gravity oscillations in a shallow water model, with applications to normal mode initialization. *Beitr. Phys. Atmos.*, **50,** 253–271.

Manabe, S., J. Smagorinsky and R. F. Strickler, 1965: Simulated climatology of a general circulation model with a hydrologic cycle. *Mon. Wea. Rev.*, **93,** 769–798.

——, J. L. Holloway, Jr. and H. M. Stone, 1970: Tropical circulation in a time-integration of a global model of the atmosphere. *J. Atmos. Sci.*, **27,** 580–613.

——, D. G. Hahn and J. L. Holloway, Jr., 1974: The seasonal variation of the tropical circulation as simulated by a global model of the atmosphere. *J. Atmos. Sci.*, **31,** 43–83.

Mass, C. F., 1979: A linear primitive equation model of African wave disturbances. *J. Atmos. Sci.*, **36,** 2075–2092.

Miyakoda, K., J. C. Sadler and G. D. Hembree, 1974: An experimental prediction of the tropical atmosphere for the case of March 1965. *Mon. Wea. Rev.*, **102,** 571–591.

——, L. Umscheid, D. H. Lee, J. Sirutis, R. Lusen and F. Pratt, 1976: The near-real-time, global, four-dimensional analysis experiment during the GATE period, Part I. *J. Atmos. Sci.*, **33,** 561–591.

——, and J. Sirutis, 1977: Comparative integrations of global models with various parameterized processes of subgrid-scale vertical transport: Description of the parameterization and preliminary results. *Beitr. Phys. Atmos.*, **50,** 445–487.

Murakami, M., 1979: Large-scale aspects of deep convective activity over the GATE area. *Mon. Wea. Rev.*, **107,** 994–1013.

Nitta, T., 1970: A study of generation and conversion of eddy

available potential energy in the tropics. *J. Meteor. Soc. Japan*, **48,** 524–528.

Norquist, D. C., E. E. Recker and R. J. Reed, 1977: The energetics of African wave disturbances as observed during Phase III of GATE. *Mon. Wea. Rev.*, **105,** 334–342.

Orlanski, I., and L. J. Polinsky, 1977: Spectral distribution of cloud cover over Africa. *J. Meteor. Soc., Japan*, **55,** 483–493.

Pasch, R., T. N. Krishnamurti and C. Depradine, 1978: An atlas of the motion field over the GATE area, Part II (250 mb). Rep. No. 8-3, Dept. Meteor., Florida State University, Tallahassee, 133 pp.

Pedgley, D. E., and T. N. Krishnamurti, 1976: Structure and behavior of a monsoon cyclone over West Africa. *Mon. Wea. Rev.*, **104,** 149–167.

Reed, R. J., and E. E. Recker, 1971: Structure and properties of synoptic-scale wave disturbances in the equatorial western Pacific. *J. Atmos. Sci.*, **28,** 1117–1133.

——, D. C. Norquist and E. E. Recker, 1977: The structure and properties of African wave disturbances as observed during Phase III of GATE. *Mon. Wea. Rev.*, **105,** 317–333.

Reeves, R. W., C. F. Ropelewski and M. D. Hudlow, 1979: Relationships between large-scale motion and convective precipitation during GATE. *Mon. Wea. Rev.*, **107,** 1154–1168.

Rennick, M. A., 1976: The generation of African waves. *J. Atmos. Sci.*, **33,** 1955–1969.

Reynolds, R., 1977: Large scale (A-scale) mean features of the GATE atmosphere during Phase III. Met-O 20 Tech. Note No. 11/105, U.K. Meteorological Office.

Riehl, H., 1954: *Tropical Meteorology*. McGraw-Hill, 392 pp.

Rosenthal, S. L., 1960: A simplified linear theory of equatorial easterly waves. *J. Meteor.*, **17,** 484–488.

Sadler, J. C., 1975: The monsoon circulation and cloudiness over the GATE area. *Mon. Wea. Rev.*, **103,** 369–387.

——, and L. K. Oda, 1978: The synoptic (A) scale circulations during the third phase of GATE, 20 August–23 September, 1974. UHMET 78-02, Dept. Meteor., University of Hawaii, 41 pp.

Simmonds, I., 1978: The application of a multi-level spectral model to data assimilation. *J. Atmos. Sci.*, **35,** 1321–1339.

Simmons, A. J., 1977: A note on the instability of the African easterly jet. *J. Atmos. Sci.*, **34,** 1670–1674.

Simpson, R. H., N. Frank, D. Shideler and H. M. Johnson, 1968: Atlantic tropical disturbances, 1976. *Mon. Wea. Rev.*, **96,** 251–259.

Smith, P. J., D. G. Vincent and H. J. Edmon, 1977: The time dependence of reference pressure in limited region available potential energy budget equations. *Tellus*, **29,** 476–480.

Stout, J. E., D. W. Martin and D. N. Sikdar, 1979: Estimating GATE rainfall with geosynchronous satellite images. *Mon. Wea. Rev.*, **107,** 585–598.

Thompson, R. M., Jr., S. W. Payne, E. E. Recker and R. J. Reed, 1979: Structure and properties of synoptic-scale wave disturbances in the Intertropical Convergence Zone of the eastern Atlantic. *J. Atmos. Sci.*, **36,** 53–72.

Tripoli, G. J., and T. N. Krishnamurti, 1975: Low-level flows over the GATE area during summer 1972. *Mon. Wea. Rev.*, **103,** 197–216.

Wallace, J. M., 1971: Spectral studies of tropospheric wave disturbances in the tropical western Pacific. *Rev. Geophys. Space Phys.*, **9,** 557–612.

Woodley, W. L., A. R. Olsen, A. Herndon and V. Wiggert, 1975: Comparison of gage and radar methods of convective rain measurements. *J. Appl. Meteor.*, **14,** 909–928.

——, C. G. Griffith, J. S. Griffin and S. C. Stromatt, 1980: The inference of GATE convective rainfall from SMS-1 imagery. *J. Appl. Meteor.*, **19,** 388–408.

Yamasaki, M., 1969: Large-scale disturbances in a conditionally unstable atmosphere in low latitudes. *Pap. Meteor. Geophys.*, **20,** 289–336.

——, 1971: A further study of wave disturbances in the unstable model tropics. *J. Meteor. Soc. Japan*, **49,** 391–415.

Yanai, M., 1969: Evolution of a tropical disturbance in the Caribbean Sea region. *J. Meteor. Soc. Japan*, **46,** 86–109.